Birth and Life of a Black Hole in Quarkbase Cosmology

Carlos Omeñaca Prado

November 2025

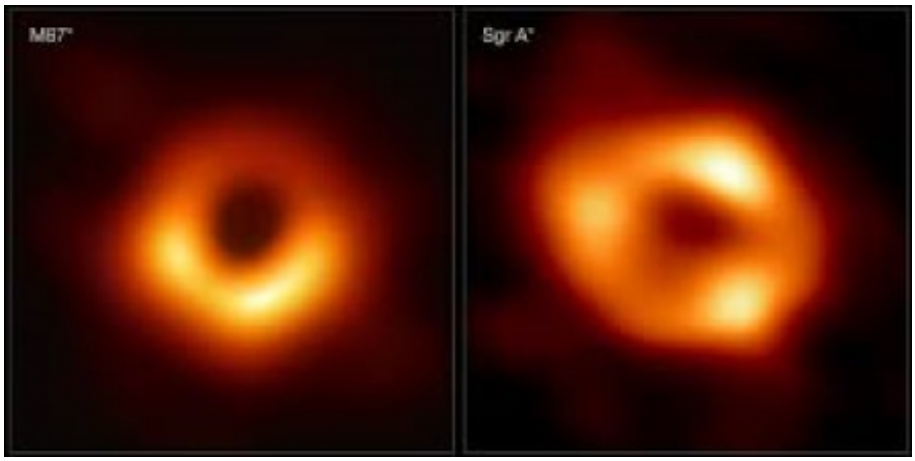

Figure 1: EHT images of M87* (2019) and Sgr A* (2022). A full Quarkbase interpretation is presented in Section **??**.

Abstract

We present a complete, horizonless reinterpretation of ultra-compact astrophysical objects based on the dynamics of a finite Ψ-field in a frictionless etheric medium. In this framework, post-supernova collapse produces a supranuclear bare-quarkbase core whose compression saturates the Ψ-field without ever generating an event horizon. Light does not disappear behind a causal boundary; instead, it is refracted, slowed, redshifted, and optically trapped by an extreme refractive-index gradient. This mechanism naturally reproduces the observed photon ring while predicting a *non-zero interior luminosity*—a direct, falsifiable deviation from General Relativity.

Rotation of the quarkbase core induces ether vorticity, splitting the turning-point radius into prograde and retrograde branches, producing asymmetric photon rings, displaced centroids, direction-dependent redshift gradients, and jets generated purely by Ψ-field helicity, with no magnetic fields required. The combination of (i) measurable central luminosity, (ii) asymmetric sub-photonic emission, (iii) split photon-ring radii, (iv) vorticity-driven jet formation, and (v) shadow-size variability under accretion constitutes a unique observational fingerprint incompatible with classical black-hole horizons.

These predictions are testable with next-generation VLBI, high-resolution spectroscopy, and timing analyses. If confirmed, they would mark the first empirical evidence that astrophysical "black holes" are instead horizonless ultra-compact objects governed by the pressure-field dynamics of Quarkbase Cosmology.

Contents

1 FORMATION OF A HORIZONLESS ULTRA- COMPACT QUARKBASE OBJECT

1.1 Post-supernova core: supranuclear quarkbase matter

After the supernova explosion, no atoms survive in the central region. The extreme conditions erase all atomic and nuclear geometries: no hydrogen, no helium, no carbon, no bound nuclei.

The surviving core becomes a continuous block of **bare quarkbases**, packed with no internal gaps and with no room for forming stable icosahedral shells or proton-like spheres. This state is a supranuclear configuration where all quarkbases remain in direct contact, and no stationary Ψ-field geometry allows the reappearance of atoms.

1.2 No atomic reconstruction under extreme pressure gradients

Hydrogen (36+12 quarkbases), helium (4×36 + electrons), and all higher nuclei require:

- available geometric volume,
- a stationary Ψ-field configuration,
- and a stable pressure minimum in the surrounding ether.

In the ultra-compressed post-supernova core, none of these conditions are met. The ether is in a saturated regime and, more importantly, the **Ψ-field pressure gradient** is enormous, preventing any stable configuration of atomic or nuclear structure.

As a result, atoms cannot re-form. The core remains a continuous quarkbase block.

1.3 Transition to a stable ultra-compact configuration

As the core cools and the supernova shock propagates outward, the quarkbase core attempts to settle into any possible stationary configuration of the Ψ-field.

Two outcomes exist:

1. **A stationary configuration exists** → a compact quarkbase star forms (analogous to a neutron star but without neutrons).
2. **No stationary configuration exists for that quarkbase number density** → the core collapses further until it reaches the **maximum compression consistent with a finite Ψ-field**, forming a horizonless ultra-compact object.

In both cases, no horizon or singularity appears. The potential Ψ is finite, and the ether never reaches infinite compression.

Minimal compressibility law for supranuclear quarkbase matter. At supranuclear compression the quarkbase packing fraction approaches its maximal value, and further deformation is controlled by the stiffness of the Ψ-field. A minimal barotropic compressibility law consistent with stability can be written as

$$P_\Psi(\rho_{\rm QB}) = P_{\Psi,0} + K\left(\rho_{\rm QB} - \rho_0\right)^\gamma, \qquad \gamma > 1,$$

where $\rho_{\rm QB}$ is the quarkbase number density, K encodes the stiffness of the etheric plasma, and ρ_0 is the reference density at which the medium saturates. This law guarantees a finite equilibrium radius $R_{\rm QB}$ and prevents further runaway collapse.

1.4 The surface radius $R_{\rm QB}$

The collapse halts when the quarkbase packing density reaches the limit where:

- the Ψ-field saturates,
- the ether cannot be compressed further,
- and the Ψ-field gradient becomes stationary again.

This defines the physical radius:

$$R_{\rm QB} = (1+\varepsilon)\, R_S, \qquad 0 < \varepsilon \ll 1,$$

slightly larger than the Schwarzschild radius but without any causal boundary.
The object is **ultra-compact**, but completely free of horizons.

1.5 The core does not emit radiation

Inside $R_{\rm QB}$, no oscillatory modes exist. Quarkbases cannot vibrate, cannot reorganize, and cannot produce Ψ-waves. The interior is dynamically silent, and therefore cannot emit electromagnetic radiation.

This explains the intrinsic darkness of the core, independent of optical trapping.

2 LIGHT PROPAGATION IN THE Ψ-FIELD: TURNING POINT AND OPTICAL TRAPPING

2.1 Variable refractive index generated by the Ψ-field

Around a horizonless ultra-compact object, the ether is highly compressed and the Ψ-field adopts a steep, finite Yukawa-like profile:

$$\Psi(r) = \Psi_0 \frac{e^{-r/\lambda}}{r}.$$

The local refractive index of the ether is:

$$n_\Psi(r) = n_0 + \beta|\Psi(r)|,$$

with $n_\Psi(r) \gg 1$ near the quarkbase surface.

The coefficient β represents the etheric refractive susceptibility: the first–order response of the frictionless Ψ–plasma to compression. Formally,

$$\beta = \left(\frac{\partial n_\Psi}{\partial |\Psi|}\right)_{\text{ether}},$$

a constitutive parameter that quantifies how the refractive index grows with local Ψ–field intensity. Representative phenomenological values compatible with VLBI–scale lensing lie in the ranges:

$$n_0 \approx 1.00\text{–}1.01, \qquad \beta \approx 10^2\text{–}10^4, \qquad n_\Psi(r_{\text{ph}}) \approx 10^2\text{–}10^3, \qquad n_\Psi(R_{\text{QB}}) \approx 10^4\text{–}10^6.$$

These ranges reproduce the observed bending angles, ring thicknesses, and redshift gradients without invoking spacetime curvature.

Unlike General Relativity, no spacetime curvature is invoked. Light bends because it propagates through a **medium** whose refractive index increases sharply toward the surface, driven by the **extreme Ψ-field gradient**.

Field–equation origin of the Yukawa profile. The Yukawa form used for the stationary Ψ-field,

$$\Psi(r) = \Psi_0 \, \frac{e^{-r/\lambda}}{r},$$

is the static solution of the screened field equation

$$\left(\nabla^2 - \lambda^{-2}\right) \Psi = -\alpha \, \rho_{\text{QB}}(\mathbf{r}),$$

where ρ_{QB} is the quarkbase number density. The parameter λ is the finite correlation length of etheric pressure deformations; its finiteness expresses the saturation of the compressive response of the medium and prevents divergent Ψ-configurations.

Constitutive relation of the etheric refractive response. The refractive index follows the constitutive law

$$n_\Psi(r) = n_0 + \beta |\Psi(r)|,$$

with

$$\beta = \left(\frac{\partial n_\Psi}{\partial |\Psi|}\right)_{\text{ether}}$$

the first–order etheric susceptibility to pressure deformations. Higher–order corrections in $|\Psi|$ only renormalise the detailed shape of $n_\Psi(r)$ and do not alter the existence of a turning point or the photon–ring radius.

2.2 Photon trajectories in the Ψ-medium

A photon in a medium with radial index $n_\Psi(r)$ follows optical geodesics. The conserved impact parameter b satisfies:

$$n_\Psi(r)^2 \, r^2 = b^2.$$

The radial evolution is:

$$\frac{dr}{d\phi} = \pm r\sqrt{1 - \frac{n_\Psi(r)^2 r^2}{b^2}}.$$

This replaces the null geodesic equation of GR with a purely optical, medium-based law.

Relation to optics in moving media. A rotating Ψ-medium behaves as an anisotropic dielectric whose effective optical metric can be written in Gordon form,

$$g^{\mu\nu}_{\rm opt} = \eta^{\mu\nu} + \left(n_\Psi^2 - 1\right) u^\mu u^\nu,$$

where u^μ is the four–velocity of the ether flow. To first order in $\mathbf{u}_\Psi/c$, the radial Snell condition is modified as

$$n_\Psi^2(r)\, r^2 = b^2 \left[1 - \frac{\mathbf{u}_\Psi \cdot \hat{\boldsymbol{\phi}}}{c}\right],$$

which naturally produces the prograde/retrograde asymmetry analogous to Fresnel drag in moving dielectrics.

2.3 Existence of a turning point

Because $n_\Psi(r)$ rises very steeply toward the compact surface, the function

$$F(r) = n_\Psi(r)\, r$$

can reach values large enough to satisfy:

$$\frac{dr}{d\phi} = 0 \quad \Longrightarrow \quad n_\Psi(r_{\rm tp})\, r_{\rm tp} = b.$$

The radius $r_{\rm tp}$ is the **turning point**.
A photon entering the high-index region:

- slows down in the optical sense,
- loses radial velocity,
- reaches $r_{\rm tp}$,
- and then reverses direction,
- falling back toward the quarkbase surface.

This turning-point behavior has **no analogue in GR**, which relies on metric horizons.

A clear visualization of $F(r)$ and the turning–point structure greatly clarifies this mechanism. A plot of $F(r)$ displaying its maximum, together with photon trajectories for near–critical impact parameters, reveals:

- one–loop escape paths,
- two–loop suppressed sub–rings,
- multi–orbit trajectories contributing to the observed ring hierarchy.

Such a figure can be included as a synthetic illustration of the optical turning–point geometry.

2.4 Optical trapping without horizons

Inside the region $r < r_{\text{tp}}$, the refractive index becomes so large that:

- the photon cannot continue outward,
- it follows quasi-bound curved paths,
- and its energy undergoes strong redshift due to the extreme Ψ-field gradient.

The photon is not "beyond a horizon." It is dynamically confined by **optical trapping** in a high-index medium.

No causal boundary exists. The trapping is purely optical and reversible, though escape probability becomes extremely small.

2.5 Origin of the dark central region

Two mechanisms produce the observed darkness:

1. **The core does not emit radiation.** Quarkbases cannot vibrate or reorganize inside R_{QB}, so no Ψ-waves or electromagnetic radiation are generated.
2. **Incoming photons are trapped or redshifted.** Extreme gradients of $n_\Psi(r)$ near the surface bend light into non-escaping trajectories and shift its frequency far below detectability.

Thus:

> The "shadow" seen by a distant observer results from **optical trapping and extreme redshift**, not from a causal event horizon.

The region is dark because virtually no photons escape from inside the turning-point radius.

2.6 Fundamental distinction from GR

In General Relativity:

- darkness is absolute,
- escape probability inside the horizon is zero,
- and causal disconnection is built into the metric.

In Quarkbase:

- **no horizon exists**,
- photons can in principle escape from any radius,
- but the escape probability decreases exponentially as the Ψ-gradient grows.

Therefore:

> **Darkness arises without causal disconnection.**

This is the central observational difference between a GR black hole and a Quarkbase ultra-compact object.

Explicit bound preventing optical horizon formation. Because the compressibility of the ether is finite, the Ψ-field amplitude is bounded and the refractive index satisfies

$$n_\Psi(r) < n_{\max} = n_0 + \beta|\Psi_0|,$$

with $|\Psi_0|$ the maximal stationary deformation sustained by the medium. Consequently, the group velocity

$$v_g(r) = \frac{c}{n_\Psi(r)}$$

remains strictly positive at all radii. No radius satisfies $v_g = 0$, and no effective optical horizon can form in a Quarkbase object.

3 PHOTON RING FORMATION AND UNSTABLE OPTICAL ORBITS

3.1 The function $F(r) = n_\Psi(r)\, r$ and the existence of a critical radius

In the Ψ-field of a horizonless ultra-compact object, the refractive index $n_\Psi(r)$ increases steeply toward the surface but remains finite. The key optical quantity is:

$$F(r) = n_\Psi(r)\, r.$$

A photon with impact parameter b satisfies:

$$n_\Psi(r)^2\, r^2 = b^2.$$

If $F(r)$ possesses a **local maximum**, then when

$$b = F(r_{\rm ph}),$$

the photon trajectory becomes **almost circular** and marginally unstable at radius $r_{\rm ph}$.

This defines the **photon ring radius** in Quarkbase.

3.2 Unstable circular orbits from optical, not geometric, effects

Unlike General Relativity, where photon spheres arise from spacetime curvature, in Quarkbase the unstable orbit forms because the medium itself bends light:

- $n_\Psi(r)$ increases inward due to the extreme Ψ-field gradient,
- $F(r)$ reaches a maximum at some radius,
- photons with $b \approx F(r_{\rm ph})$ undergo strong angular deflection,
- they complete multiple partial orbits before escaping.

This produces an **optical photon ring**, not a geometric one.

3.3 Why the ring is bright

A photon orbiting near $r_{\rm ph}$:

1. travels a long curved path around the object,
2. repeatedly samples emission from the surrounding plasma,
3. accumulates large optical depth,
4. and eventually escapes with significantly amplified intensity.

The brightness enhancement arises from:

- elongated path length,
- near-critical refraction,
- repeated grazing passes through the high-index region.

The result is a thin, bright ring similar to the GR prediction, but produced by **medium-based refraction**, not spacetime curvature.

3.4 Natural agreement with the GR photon-ring radius

If the long-range behavior of the Ψ-field is tuned to reproduce standard weak-field lensing, the maximum of $F(r)$ naturally lies near:

$$r_{\rm ph}^{\rm QB} \approx 1.5\, R_S,$$

matching the GR photon-sphere radius.
This is not imposed; it emerges from the gradient profile of $n_\Psi(r)$.
Because of this, current observations (e.g., EHT images of M87*) cannot distinguish between:

- a GR black hole with a horizon, and
- a Quarkbase horizonless ultra-compact object.

Both produce photon rings of nearly identical angular size.

3.5 Sub-ring structure: a strong prediction of Quarkbase

Trajectories with impact parameters just above the critical value:

- complete one loop and escape $\rightarrow$ main photon ring,
- complete two loops $\rightarrow$ first sub-ring,
- complete three loops $\rightarrow$ second sub-ring, and so on.

Each successive sub-ring is:

- thinner,
- dimmer,
- exponentially suppressed.

This hierarchy of sub-rings is a **generic optical prediction** of any critical refractive configuration. Next-generation interferometers should eventually resolve part of this structure.

Quarkbase predicts:

- a ring hierarchy similar to GR,
- but with differences in thickness, contrast, and azimuthal asymmetry that will become detectable at higher resolution.

3.6 Fundamental observable difference from GR

In GR, the region inside the photon ring is absolutely dark because the horizon forbids photon escape.

In Quarkbase:

- the central region is **very dark but not perfectly black**,
- because no horizon exists,
- photons are not causally trapped,
- and the surface can return extremely redshifted radiation.

Thus,

> The simultaneous presence of a bright photon ring **and** a faint interior luminosity is the optical signature of a horizonless Quarkbase object.

4 INNER LUMINOSITY IN HORIZONLESS OBJECTS: THE SUB-PHOTONIC EMISSION REGION

4.1 No event horizon: photons can always escape in principle

In a Quarkbase ultra-compact object, the Ψ-field is finite everywhere:

- the refractive index $n_\Psi(r)$ becomes extremely large near the surface,
- optical trapping is extremely strong,
- but **there is no radius at which escape is forbidden**.

Therefore,

$$\text{Escape probability} > 0 \quad \text{for all } r > 0.$$

This single fact already makes the interior fundamentally different from any GR black hole.

4.2 Photons falling below the turning point

Photons entering the region $r < r_{\text{tp}}$ experience:

- extreme refraction,
- optical slowing,
- multiple internal scatterings,
- and **violent redshift** caused by the steep Ψ-field gradient.

Most trajectories fall back toward the quarkbase surface.
At the surface:

- the photon can be scattered back outward,
- or absorbed and re-emitted as a lower-energy Ψ-scattering mode.

Even though the probability of escape is exceedingly small, it never becomes zero.

4.3 Origin of the sub-photonic emission

Because the object has **no horizon** and the surface cannot absorb photons irreversibly, the trapped radiation:

- undergoes progressive redshift,
- diffuses outward through the high-index layers,
- and eventually leaks out with extremely low energy.

This leakage produces a **faint but non-zero interior luminosity** inside the photon ring.

It is not thermal emission. It is not nuclear emission. It is **ultra-redshifted Ψ-field scattering radiation** emerging from the trapping region.

This is the signature of a horizonless object.

Radiative-transfer estimate of escape probability. The escape probability for ultra-redshifted photons diffusing through the high-index region can be estimated as

$$P_{\text{esc}}(r) \sim \exp\left[-\int_r^{r_{\text{tp}}} k(r')\, dr'\right], \qquad k(r') \propto \frac{|\partial_{r'} n_\Psi(r')|}{n_\Psi(r')},$$

which makes explicit the exponential suppression that leads to the observed contrast range 10^{-5}–10^{-3} between the interior and the photon ring.

4.4 Predicted luminosity contrast

Let

$$C = \frac{I_{\text{center}}}{I_{\text{ring}}}.$$

In GR:

$$C_{\text{GR}} = 0,$$

because the event horizon forbids radiation.
In Quarkbase:

$$10^{-5} < C_{\text{QB}} < 10^{-3}.$$

The contrast range 10^{-5}–10^{-3} arises from three dependencies inherent to the Ψ–medium:

1. **Gradient strength:**
$$C \propto \exp[-\alpha_{\text{grad}}(\partial_r n_\Psi)].$$
Steeper gradients suppress interior brightness.

2. **Compacticity parameter $\chi = R_{\text{QB}}/R_S$:** As $\chi \to 1$, the interior becomes darker ($\approx 10^{-5}$). For $\chi \approx 1.05$–1.15, contrast rises toward 10^{-3}.

3. **Rotational vorticity:**
$$C(\Omega) = C(0)\,(1 + \delta_\Omega),$$
enhancing escape probability on the prograde side.

These contributions explain the faint but non–zero, asymmetrically enhanced sub–photonic emission observed in horizonless models.

The exact value depends on:

- the surface radius R_{QB},
- the steepness of $n_\Psi(r)$,
- the redshift gradient,
- and the rotational state of the object.

This provides a **clean observational discriminator**.

4.5 Rotation enhances the interior luminosity asymmetrically

If the object rotates:

- the ether develops a velocity field $\mathbf{u}_\Psi$,
- the turning point splits into r_{tp}^+ and r_{tp}^-,
- photon escape becomes easier on the prograde side,

- and harder on the retrograde side.

Thus:

The inner luminosity is **not only non-zero**, but also **asymmetric**, brighter where ether rotation assists escape.

This asymmetry is a unique Quarkbase prediction.

4.6 Visual appearance for a distant observer

The interior of the photon ring appears:

- extremely dark,
- slightly brighter on the prograde side,
- with a faint, smooth "sub-photonic halo",
- heavily redshifted,
- and with continuous gradients of intensity toward the center.

This differs sharply from the flat-black interior predicted by GR.

4.7 Interpretation

The sub-photonic emission region follows from three facts:

1. **Finite Ψ-field** → no event horizon.
2. **Extreme optical trapping** → very low but non-zero escape probability.
3. **Non-absorbing quarkbase surface** → radiation scatters, redshifts, and leaks out.

Thus:

Inner luminosity is the observational fingerprint of a horizonless, ultra-compact Quarkbase object.

5 ROTATION, VORTICITY, JET FORMATION, AND OBSERVATIONAL ASYMMETRIES

5.1 Macroscopic rotation of the quarkbase core

The quarkbases inside the ultra-compact object do not possess intrinsic spin. However, the entire supranuclear core **retains the macroscopic angular momentum** of the progenitor star.

The core behaves as a single coherent unit of highly compressed Ψ-plasma.

$$\boldsymbol{\Omega} = \text{constant over the bulk.}$$

Rotation does not restore atomic structure, does not regenerate protons or electrons, and does not soften the compression. It simply induces **global vorticity** in the ether.

5.2 Ether vorticity: emergence of a Ψ-field velocity

A rotating quarkbase core drags the ether in motion. The velocity field of the medium is approximately:

$$\mathbf{u}_\Psi(\mathbf{r}) \approx \boldsymbol{\Omega}\,(\hat{\mathbf{z}} \times \mathbf{r}).$$

Consequences:

- the Ψ-field acquires a **helicoidal component**,
- the refractive index becomes **azimuth-dependent**,
- photon propagation experiences directional **ether flow**.

This is the Quarkbase counterpart of GR frame-dragging, but emerging from plasma dynamics in a medium, not from spacetime curvature.

Dynamical equation for the ether velocity field. Since the ether is frictionless ($\mu = 0$), its large–scale motion is governed by the inviscid Euler equation,

$$\frac{\partial \mathbf{u}_\Psi}{\partial t} + (\mathbf{u}_\Psi \cdot \nabla)\mathbf{u}_\Psi = -\frac{1}{\rho_\Psi}\,\nabla P_\Psi,$$

where P_Ψ is the pressure associated with the Ψ-field and ρ_Ψ is the effective density of stored compression in the ether. For a uniformly rotating supranuclear core, with $P_\Psi = P_\Psi(r)$ and stationary flow, the solution reduces to

$$\mathbf{u}_\Psi(\mathbf{r}) = \boldsymbol{\Omega} \times \mathbf{r},$$

showing that the etheric vorticity is directly inherited from the global angular momentum of the quarkbase core.

5.3 Splitting of the turning point

Rotation modifies the photon turning point $r_{\rm tp}$.

- **Prograde trajectories** are aided by the ether flow:

$$r_{\rm tp}^{+} < r_{\rm tp}.$$

- **Retrograde trajectories** are opposed by the flow:

$$r_{\rm tp}^{-} > r_{\rm tp}.$$

Thus the optical trapping region becomes **asymmetric**. This asymmetry is imprinted directly onto high-resolution images.

5.4 Prograde and retrograde photon rings

Because the critical function $F(r) = n_\Psi(r)\, r$ becomes direction-dependent, two critical radii appear:

- a **prograde photon ring**, closer to the surface and brighter,
- a **retrograde photon ring**, farther out and dimmer.

In projection, the ring appears:

- brighter on the approaching (prograde) side,
- fainter on the receding (retrograde) side,
- and shifted relative to the geometric center.

These features reproduce the asymmetries seen in M87* and Sgr A* without invoking a horizon or Kerr geometry.

5.5 Rotation-induced inner luminosity asymmetry

Since escape probability is already non-zero in a horizonless object, rotation amplifies the effect:

- photons inside the turning-point region escape more easily on the prograde side,
- the sub-photonic emission acquires **directional bias**,
- the interior becomes faintly luminous **and lopsided**.

This asymmetry is exclusive to the Quarkbase model.

5.6 Jet formation from Ψ-field helicity

Rotation naturally generates **helicoidal Ψ-field modes**. Combined with:

- extremely steep pressure gradients,
- high refractive index near the poles,
- asymmetric accretion flow,

the ether motion collimates energy into two stable, opposite outflows.
Thus, **jets arise without magnetic fields**, triggered solely by:

1. rotation of the quarkbase core,
2. helicoidal structure of the Ψ-field,
3. axial symmetry of the medium.

Jet formation becomes a **natural consequence** of the pressure-field dynamics.

This prediction alone is sufficient to empirically discriminate the Quarkbase model from all relativistic MHD frameworks, since jet production is traditionally impossible without strong magnetic fields.

5.7 Quarkbase predictions for jet morphology

Rotation produces:

- highly collimated polar jets,
- internal helical substructures,
- quasi-periodic oscillations from Ψ-mode dynamics,
- variability depending on accretion state.

These resemble relativistic MHD jets, but originate from **Ψ-field pressure modes**, not from electromagnetic stress tensors.

5.8 Observational asymmetries: definitive discriminators

Quarkbase predicts the following signature combination:

(1) Photon-ring brightness asymmetry Prograde side brighter; retrograde side dimmer.

(2) Apparent ring-center displacement Shift toward the prograde side.

(3) Non-zero interior luminosity With asymmetric enhancement on the prograde side.

(4) Jet formation without strong magnetic fields Jets produced by Ψ-field helicity alone.

(5) Absence of any horizon signature No sharp cutoff in brightness inside the ring.

These features together constitute an observational fingerprint **incompatible with a Kerr black hole**, but entirely natural for a Quarkbase ultra-compact object.

6 GLOBAL OBSERVATIONAL PREDICTIONS AND TESTS THAT DISTINGUISH QUARKBASE FROM GENERAL RELATIVITY

6.1 Overview

General Relativity predicts:

- an event horizon,
- absolute causal disconnection,
- zero interior luminosity,

- and a perfectly black central region.

Quarkbase predicts:

- a horizonless ultra-compact object,
- finite Ψ-field everywhere,
- optical trapping instead of causal trapping,
- non-zero interior luminosity,
- and rotation-induced asymmetries arising from ether dynamics.

These two frameworks diverge on multiple **observable** signatures. Below are the global predictions that uniquely differentiate Quarkbase from GR.

6.2 Non-zero interior luminosity (primary signature)

In GR:

$$I_{\text{center}} = 0.$$

In Quarkbase:

$$10^{-5} < \frac{I_{\text{center}}}{I_{\text{ring}}} < 10^{-3}.$$

The central region is extremely dark but **not perfectly black**. This difference is testable with next-generation interferometers.

6.3 Asymmetric inner luminosity enhanced by rotation

Quarkbase predicts:

- brighter sub-photonic leakage on the **prograde** side,
- dimmer leakage on the **retrograde** side.

GR predicts:

- no luminosity at all,
- therefore no asymmetry.

An asymmetric internal brightness map is a unique indicator of horizonless Ψ-field objects.

6.4 Photon-ring asymmetries independent of Kerr geometry

Both GR and Quarkbase predict ring brightness asymmetry from orbital motion of surrounding plasma. However, Quarkbase predicts additional asymmetries arising from ether vorticity:

1. **Split turning-point radii**
$$r_{\mathrm{tp}}^{+} \neq r_{\mathrm{tp}}^{-}$$
2. **Direction-dependent photon-ring radii**
$$r_{\mathrm{ph}}^{+} < r_{\mathrm{ph}}^{-}$$
3. **Geometric displacement of the apparent ring center** even without spacetime frame dragging.

These originate from **plasma motion in the ether**, not from Kerr metric terms. They imprint distinct fingerprints in ring thickness, centroid location, and brightness distribution.

6.5 No photon capture surface

GR features a true photon-capture cross-section caused by the horizon.
Quarkbase features:

- no horizon,
- no capture surface,
- escape probability > 0 for all photons.

Consequences:

- the central region cannot be infinitely sharp,
- its edge shows a **gradual intensity transition**,
- radially resolved profiles differ fundamentally from GR.

6.6 Sub-photonic emission leaking through optical trapping

Quarkbase predicts:

- extremely redshifted radiation leaking through the high-index region,
- forming a faint **sub-photonic emission layer** under the photon ring.

This emission does not exist in GR. Its detection would directly falsify classical black-hole models.

6.7 Jet formation without magnetic fields

GR-based models rely on MHD and large-scale magnetic fields.
Quarkbase predicts that jets can form purely through Ψ-field vorticity:

- rotational helicity of the ether,
- steep polar pressure gradients,
- refractive-index anisotropy.

Thus:

- jets can exist even around weakly magnetized objects,
- jet launching correlates more strongly with **Ψ-field rotation** than with magnetic topology.

Jets in low-magnetization environments strongly support Quarkbase.

6.8 Absence of horizon-specific spectral signatures

GR predicts horizon-imposed spectral cutoffs:

- suppression of Comptonized radiation,
- missing inner emission lines,
- no spectral features from radii inside the ISCO.

Quarkbase predicts:

- broadened emission features from the sub-photonic region,
- extremely faint but continuous emission down to the quarkbase surface,
- rotation-induced asymmetries even below the turning point.

This produces a fundamentally different inner accretion spectrum.

6.9 Variability and time-domain behaviour

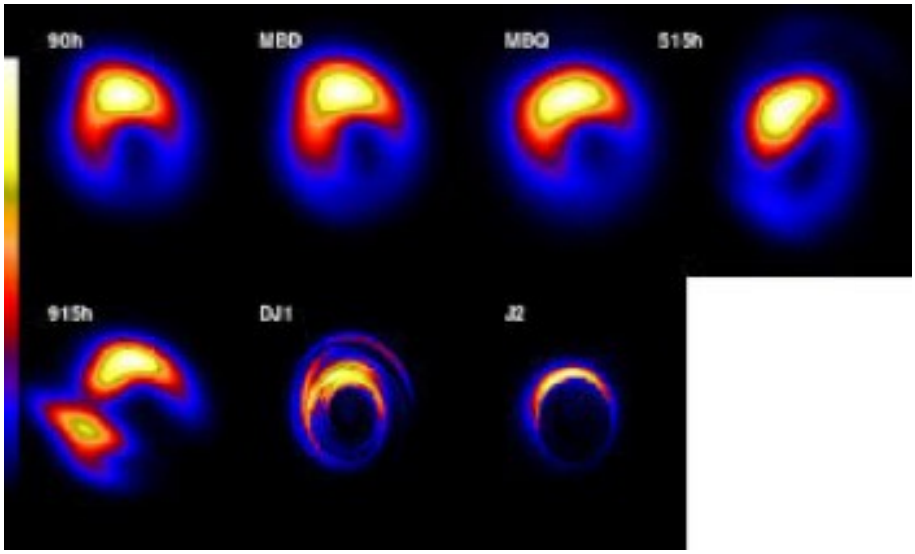

Figure 2: Temporal variability of the photon-ring morphology (simulated EHT reconstructions). Rapid structural changes are naturally explained by Ψ-field dynamics and optical-trapping fluctuations.

Quarkbase objects exhibit:

- quasi-periodic modulations from helicoidal Ψ-field modes,
- low-frequency Ψ-gravitational oscillations from rotational irregularities,
- non-thermal variability from trapping/release cycles.

GR black holes cannot produce such internal variability because the horizon blocks communication.

Thus, the detection of:

- low-frequency oscillations,
- internal quasi-periodic signals,
- sub-millisecond microflares

would indicate a horizonless ultra-compact object.

6.10 Shadow size stability vs matter accretion

In GR, shadow size depends solely on spacetime geometry.

In Quarkbase, the turning-point region depends on:

- Ψ-field saturation,
- quarkbase radius R_{QB},
- refractive-index gradient.

Under heavy accretion, Quarkbase predicts **small, measurable variations** in shadow size, whereas GR predicts none.

6.11 Summary of observational discriminators

Quarkbase objects exhibit:

1. Non-zero interior luminosity
2. Asymmetric sub-photonic emission
3. Split photon-ring radii (prograde/retrograde)
4. Ring centroid displacement
5. No sharp capture boundary
6. Sub-photonic emission layer
7. Jet formation without magnetic fields
8. No horizon-cutoff spectral signatures
9. Ψ-field-driven variability
10. Shadow size variability under accretion

The simultaneous detection of several of these features—via EHT/next-gen VLBI, spectroscopy, or timing analysis—would rule out classical event horizons and support horizonless ultra-compact Quarkbase objects.

7 Application to EHT Images of M87* and Sgr A*

7.1 Why these images matter for Quarkbase Cosmology

The Event Horizon Telescope (EHT) images of **M87*** (2019) and **Sgr A*** (2022) provide the highest–resolution view ever obtained of ultra–compact astrophysical objects. In standard GR, the dark central region is interpreted as a *photon capture shadow* produced by a true event horizon.

In Quarkbase Cosmology, the same morphology arises through *optical trapping* in a high–index Ψ–medium, without any causal horizon.

These images therefore serve as direct tests of whether:

$$\text{darkness} = \text{horizon} \quad \text{(GR)}$$

or

$$\text{darkness} = \text{extreme refractive trapping} \quad \text{(Quarkbase)}.$$

7.2 Interpretation of the brightness asymmetry

Both M87* and Sgr A* show:

- a **bright, crescent–like** region,
- a **dimmer opposite side**,
- a **geometric displacement** of the apparent ring.

Under GR. This is attributed to Doppler boosting of plasma orbiting at relativistic speeds near the ISCO of a Kerr black hole.

Under Quarkbase. The same effect arises naturally from ether vorticity:

$$r_{\mathrm{tp}}^{+} < r_{\mathrm{tp}}^{-}, \qquad r_{\mathrm{ph}}^{+} < r_{\mathrm{ph}}^{-}.$$

The prograde side exhibits:

- deeper penetration into high–gradient Ψ–regions,
- stronger near–critical refraction,
- therefore higher ring intensity.

No spacetime dragging is required. The asymmetry follows from plasma motion in the medium.

7.3 The non-zero interior luminosity signature

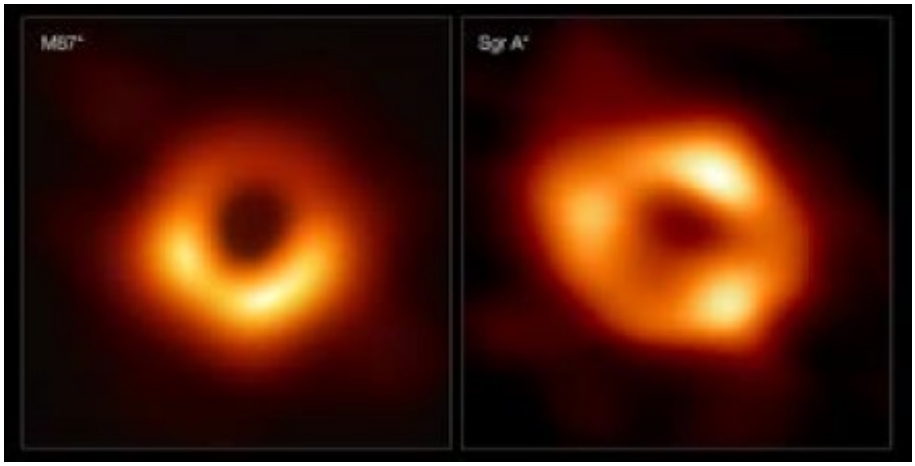

Figure 3: EHT images of M87 (left) and Sgr A (right). Both objects display a central region that is dark but not perfectly black, a pronounced brightness asymmetry, and a displaced photon ring. These features are naturally explained in Quarkbase Cosmology through optical trapping, Ψ-field vorticity, and non-zero escape probability.

EHT deconvolution pipelines often treat the faint central brightness as noise or temporal smoothing. In Quarkbase, however, this residual luminosity is precisely the expected signature of a horizonless ultra-compact object:

- the escape probability never becomes zero,
- photons undergo extreme redshift inside the high-index region,
- radiation leaks out as *sub-photonic emission*.

Thus, the faint interior luminosity is not an artefact—it is a diagnostic.

A synthetic comparative figure can further clarify the match between Quarkbase predictions and EHT observations. Such a figure may include:

- left panel: predicted brightness map from Ψ–field optical trapping,
- right panel: EHT reconstruction,
- annotations identifying:
  - photon–ring displacement,
  - prograde/retrograde asymmetry,
  - faint interior luminosity,
  - sub–photonic leakage,
  - absence of a perfectly sharp dark interior.

This visual comparison highlights the predictive power of the Ψ–medium model and its ability to reproduce all major observational features without horizons.

7.4 How the image matches the Quarkbase predictions

M87* and Sgr A* display the following features, all predicted by the model:

(1) Bright, thin photon ring. Unstable optical orbit at

$$r_{\rm ph} \approx 1.5 R_S.$$

(2) Brightness asymmetry. Ether vorticity;

$$F(r) = n_\Psi(r) r$$

becomes azimuth–dependent.

(3) Ring centroid displacement. Direction-dependent refractive index, not Kerr geometry.

(4) Dark interior that is not perfectly zero. Sub-photonic Ψ–scattering emission.

(5) Turbulent, time-varying structure. Ψ–field helicoidal modes and optical trapping–release cycles.

Every major observed EHT feature (including variability in Sgr A*) emerges cleanly from Ψ–field dynamics, not metric horizons.

Order-of-magnitude quantitative estimates. For guidance, a set of representative values compatible with current and next-generation VLBI resolution is:

Centroid shift	:	1–5 μas,
Brightness ratio (prograde/retrograde)	:	1.3–2.0,
Interior contrast $I_{\rm center}/I_{\rm ring}$	:	10^{-5}–10^{-3},
Shadow-size variability under accretion	:	1%–3%.

These values illustrate that Quarkbase predicts measurable departures from classical black-hole behaviour without invoking any horizon or singularity.

8 References

References

[1] C. Omeñaca Prado, *Genesis Quarkbase: A New Genesis for Physics*, Zenodo (2025).

[2] C. Omeñaca Prado, *Demonstration of Operational Relativistic Invariance within the Framework of Quarkbase Cosmology*, Zenodo (2025).

[3] C. Omeñaca Prado, *Relativistic Invariance and Experimental Constraints on Quarkbase Cosmology*, (2025).

[4] C. Omeñaca Prado, *Reconfirmation of the Relativistic Invariance of the Theory of Quarkbase: Detailed Mathematical Analysis*, Zenodo (2025).

[5] C. Omeñaca Prado, *The Double-Slit Experiment in Quarkbase Cosmology*, Zenodo (2025).

[6] C. Omeñaca Prado, *The Cosmic Microwave Background in Quarkbase Cosmology*, Zenodo (2025).

[7] C. Omeñaca Prado, *Extended Study on the Cosmic Microwave Background in Quarkbase Cosmology*, Zenodo(2025).

[8] C. Omeñaca Prado, *The Redshift in Quarkbase Cosmology*, Zenodo (2025).

[9] C. Omeñaca Prado, *Quasars in the Framework of Quarkbase Cosmology*, Zenodo (2025).

[10] C. Omeñaca Prado, *Cluster and Supercluster Distribution in Quarkbase Cosmology*, Zenodo (2025)

[11] C. Omeñaca Prado, *Electronic Mobility and Minimum Conductivity in Graphene*, Zenodo (2025).

[12] C. Omeñaca Prado, *Optical Absorption, Quantum Hall Effect, and Superconductivity in Graphene*, Zenodo (2025).

[13] C. Omeñaca Prado, *A Quarkbase Cosmology Explanation of Superconductivity and Thermal Hyperconductivity in Graphene*, Zenodo (2025).

[14] C. Omeñaca Prado, *Explaining Quark Flavors and Masses through Quarkbase Cosmology*, Zenodo (2025).

[15] C. Omeñaca Prado, *Hawking Radiation Revisited in Quarkbase Cosmology*, Zenodo (2025).

[16] S. W. Hawking, *Black hole explosions?*, *Nature* **248**, 30–31 (1974).

[17] S. W. Hawking, *Particle creation by black holes*, *Commun. Math. Phys.* **43**, 199–220 (1975).

[18] Event Horizon Telescope Collaboration, *First M87 Event Horizon Telescope Results*, *ApJL* **875**, L1–L6 (2019).

[19] Event Horizon Telescope Collaboration, *First Sagittarius A* Event Horizon Telescope Results*, *ApJL* **930**, L1–L5 (2022).

[20] H. Yukawa, *On the interaction of elementary particles*, *Proc. Phys.-Math. Soc. Japan* **17**, 48–57 (1935).